Kinematics of helical flow between concentric cylinders with axial through flow

M. El El Hassan, V. Sobolik, A. Chamkha, Magdalena Kristiawan

International Journal of Heat and Mass Transfer 182 (2022) 121938

Contents lists available at ScienceDirect

International Journal of Heat and Mass Transfer

journal homepage: www.elsevier.com/locate/hmt

Kinematics of helical flow between concentric cylinders with axial through flow

M. El Hassan [a,*], V. Sobolik [b], A. Chamkha [c], M. Kristiawan [d]

[a] Faculty of Engineeing, Prince Mohammad Bin Fahd University, Al Khobar 34754, Saudi Arabia
[b] LaSIE, UMR 7356, University of La Rochelle La Rochelle 17042, France
[c] Faculty of Engineering, Kuwait College of Science and Technology, Doha, Kuwait
[d] INRAE UR 1268, Biopolymers, Interactions and Assemblies (BIA), Nantes 44316, France

ARTICLE INFO

Article history:
Received 28 May 2021
Revised 18 August 2021
Accepted 4 September 2021
Available online 20 September 2021

ABSTRACT

Kinematical and geometrical parameters of helical vortices winding in the same (right-handed) or opposite direction (left-handed) to the base Taylor-Couette-Poiseuile flow were studied at low $Ta = R_1\ d/\nu < 319$ and $Re = U_M\ d/\nu < 10.5$ numbers. The inner cylinder ($R_1 = 24.85$ mm) rotated and the outer one ($R_2 = 30.95$ mm) was stationary. The parameters of helical vortices were obtained from flow visualizations and the wall shear rates were deduced from the electrodiffusion currents of three mass transfer probes flush mounted on the wall of the outer cylinder Kristiawan et al. [11]. The vector field of wall shear rate on the outer cylinder was reconstructed using a three-segment mass transfer probe. It is found that the axial component of the wall shear rate of the left-handed helices is greater than that of the right-handed helices. The motion of the flow structures near the outer wall was described by the velocity V resulting from the axial drifting velocity (U_D) and the azimuthal velocity W. It was shown that the axial velocity perceived by an observer or sensor fixed in the laboratory system U_{OBS} is composed of the drifting velocity U_D and the velocity due to the helix rotation U_Ω, known as Barber pole effect. New insight on the helical structures are revealed from studying the variations of different parameters such as the helix pitch p, the rotation rate and the observed angular velocity of the helices.

1. Introduction

The Couette flow between concentric cylinders induced by the rotating inner cylinder becomes instable when the Taylor number, $Ta = R_1\ \Omega\ d/\nu$, reaches a critical value. Pairs of counter rotating toroidal vortices thus form in the so-called Taylor-Couette flow (TCF). The height of a vortex cell (p) is approximately equal to the gap width (d) between the cylinders, which means that the axial wavelength is about 2 d.

Imposing an axial through flow (pressure gradient) on TCF, "helical-type" instabilities occur when the Reynolds number, $Re = U_M\ d/\nu$, attains a critical value [4,7,17]. One or several pairs of counter rotating helices appear. If the outer cylinder is at rest, the helices arise only due to the imposed axial through flow and the resulting axial velocity component has a parabolic profile. It should be noted that the helices between counter rotating cylinders occur without axial superposed pressure gradient and the velocity field has a cubic profile, i.e. the axial flow close to the inner cylinder has an opposite sign of that close to the outer cylinder [2,18].

The investigation of the flow instabilities in the Taylor-Couette-Poiseuille flow (TCPF) is interesting from both theoretical and practical points of view. For example, this type of flows is found in separation devices, journal bearing and rotating machinery [20]. Since the axial through flow decreases the torque required by rotating the inner cylinder at a given speed, understanding the TCPF with an imposed axial through flow allows to control the related flow fields.

The TCPF was previously studied from different points of view. Critical Taylor number and flow stability were studied theoretically and numerically [1,4,5,7,13,16,19]. Several experimental techniques were used: flow visualisation [3,12,17,19], electrodiffusion probes [9] and PIV technique [2,21].

Raguin and Georgiadis [15] reconstructed a velocity field corresponding to the stationary helical vortex (SHV) using experimental data obtained via magnetic resonance imaging. In their experimental set-up with the inner cylinder rotating and an axial through flow, the authors observed one pair of spirals ($n = -1$) at $Ta = 147.2$ and $Re = 11.14$, with $\eta = 0.5$. They proposed an analytical reconstruction of the three-dimensional volume-preserving duct flow

* Corresponding author.
E-mail address: melhassan@pmu.edu.sa (M.E. Hassan).

https://doi.org/10.1016/j.ijheatmasstransfer.2021.121938
0017-9310/

Nomenclature

d	gap width between cylinders
f_H	frequency of structure (passage frequency of helices)
f_C	frequency of inner cylinder rotation
l	helix lead; axial advance of a helix during one complete revolution (2π)
k_t	coefficient for characteristic time of helix passage
n	number of starts of helix pairs, number of helix pairs, number of helix on one perimeter
p	helix pitch (vortex cell height); axial wave length of toroidal Taylor vortices = $2p$
Re	Reynolds number, $Re = U_M\ d/\nu$
R_1, R_2	radius of the inner and outer cylinder
R_{ij}	correlation between currents of simple probes i and j
S	wall shear rate
Ta	Taylor number, $Ta = R_1\ \Omega\ d/\nu$
$t_{2,k}$	time shift between the current of probe 2 and current k=1 or 3
$t_{2,2}$	current period measured by probe 2
U_M	mean velocity of axial through flow
U_D	drifting velocity due to the axial through flow
U_{OBS}	axial velocity seen by an observer or probe fixed with laboratory system, $U_{OBS} = U_D + U_\Omega$
U_Ω	velocity of axial displacement of helical pattern due to rotation, Barber pole effect, $U_\Omega = l\ \Omega_H / 2\pi = R_2 \tan\alpha\ \Omega_H$
V	final structure velocity, $V^2 = U_D{}^2 + W^2$
W	azimuthal velocity, $W = \Omega_H R_2$
z	axial coordinate
α	angle between helix and plane of rotation, $\tan\alpha = l / 2\pi\ R_2 = U_\Omega / W$
β	angle between velocity vector V and its component W, $\tan\beta = U_D / W$
Ω_H	angular velocity of structure
Ω	angular velocity of inner cylinder

field and suggested that the SHV mode is a candidate for the study of particle segregation since it corresponds to a minimum in dissipation and mixing in comparison with a wide class of perturbed neighboring modes. However, no data was provided about the rotation and axial velocity of the helix.

The flow patterns of a Taylor-Couette-Poiseuille flow at low axial Reynolds and rotational Taylor numbers (Re < 10.5, Ta < 319) were studied in our previous work [11]. Cinema films of different helical patterns together with the corresponding histories of the wall shear rate components were presented. The axial and azimuthal components of the wall shear rate were measured on the outer fixed cylinder using a three-segment electrodiffusion (mass transfer) probe. Different flow structures such as Taylor vortices, helices winding in the same or opposite direction of the base flow, helices that were observed as stationary or moving in the axial direction, with or without superposed azimuthal waves were described. It was found that the wall shear stress is a function of Ta but no significant dependence on Re was observed. Complete map of flow structures in the space Ta-Re was presented.

The present paper focuses on the kinematic parameters of the helices and their imprint on the wall in term of shear rate. Two mysteries that have never been previously explained are investigated experimentally. First, the reason why the right-handed helices are seen to be stationary, i.e. the drifting velocity of the right-handed helices is equal to the axial velocity caused by the helix rotation (Barber-pole effect). Second, the reason for which the passage frequency of left-handed helices through a fix point, normalized with the rotation frequency of the inner cylinder, has integer values of 1 for Re < 10 and 2 for Re > 10. This paper also presents the wall shear rate vectors reconstructed from the mass transfer measurements using three-segment probe for the entire cycle of helical structures passing. This represents the first experimental quantitative description of both the axial and azimuthal wall shear stress components, simultaneously.

2. Theoretical analysis of the helix velocity and the wall shear rate

The number n characterizes the helix azimuthal wave number [19]. The absolute value of n gives the number of helix pair starts (number of helix in the following, $n = 1$ for one pair etc.) and the sign stands for its inclination. The positive n means that the helix inclination is opposite of that of the basic Couette-Poiseuille flow or "left-handed helix", while the negative sign corresponds to an inclination in the sense of the basic CP flow or "right-handed helix". Taylor toroidal vortices have $n = 0$. The helix inclination angle α depends on the helix lead (l) which is the axial advance of a helix during one revolution (2π). Using the analogy with a screw thread, the helix cell height is called the pitch (p). It follows that $l = 2\ |n|\ p$. Raguin and Georgiadis [15] used the name axial wavelength ($2p$) for stationary helical vortices.

Helices winding in the same (right-handed) or opposite direction (left-handed) to the base Couette- Poiseuille flow were presented in our previous paper [11]. We suggested that the helices rotate because of the inner cylinder rotation and move in the axial direction at a drifting velocity U_D induced by the imposed axial through flow. The interaction of helices with the stationary wall of the outer cylinder results in a field of wall shear rate. This field moves at the velocity V, composed of the drifting velocity U_D and an azimuthal velocity W. The velocity vectors on the unrolled wall of the outer cylinder are shown in Fig. 1. The wall is viewed from the exterior in the same way as the helices in Fig. 3. The electrodiffusion probe is denoted by the point E. The thick dashed lines represent points having the same wall shear rate, e.g. a maximum. The angle α is the helix inclination. The resulting velocity V makes the angle β with the velocity W. U_Ω is the axial velocity perceived with the eye or measured with a probe when a helix only rotates. This velocity is known as the "Barber pole effect". It depends on the angle α and the azimuthal velocity: $U_\Omega = W \bullet \tan\alpha$. When $U_D = U_\Omega$, the helix moves at the velocity V parallel with its pattern, see Figs. 1a and 3. In this case, the helix is perceived as stationary, see Film. 1.

If the angle α is different from β, the probe E measures the wall shear rates along the dashed line AE (Fig. 1b and c). When the point A passes past E, the probe measures again the maximum of wall shear rate. It means that all the history of wall shear rate during one period was acquired, see Fig. 10 in Kristiawan et al. [11]. The only exception is the case of a stationary helix when the resulting velocity V is parallel with the helix inclination angle, i.e. the angle β is equal to α. The points with the same wall shear rate then defiles past the probe E, see Fig. 9 in Kristiawan et al. [11]. The period of wall shear rate is given by the length of the line AE divided by the velocity V. For the same V (same Re and Ta), the period of the right-handed helix (Fig. 1b) is longer than that of the left-handed helix (Fig. 1c). The mathematical proof of this concept is given in the Appendix.

(a) Stationary right-handed helix (inclination is parallel with the basic CP flow, $\alpha = \beta$, n = -1),
(b) moving right-handed helix (inclination is in the sense of basic CP flow, $\alpha < \beta$, n = -1),

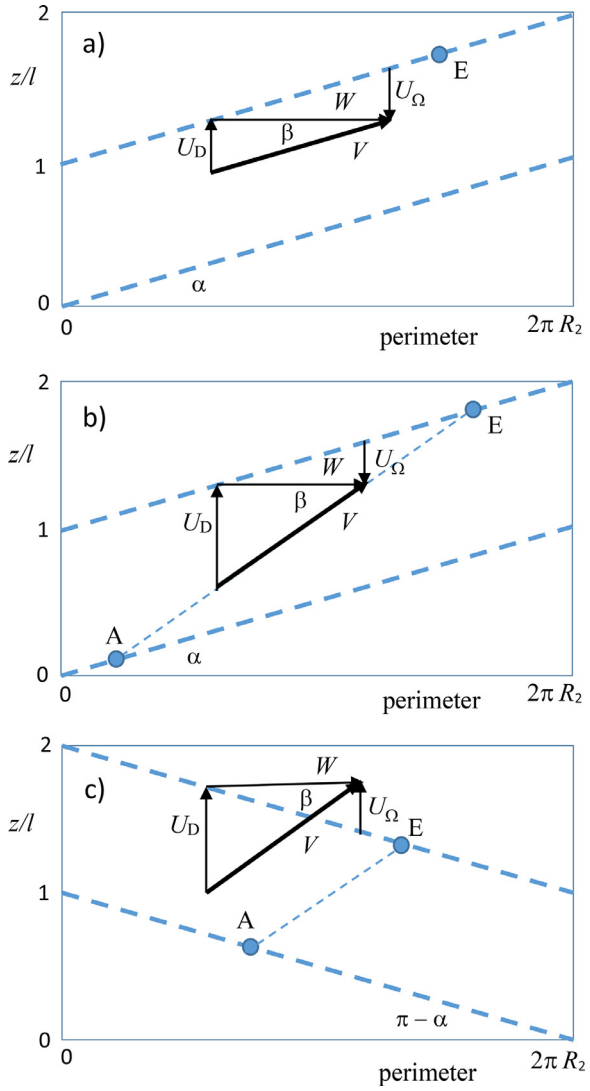

Fig. 1. Unrolled wall of the outer cylinder with velocity vectors of helix. z/l is the axial coordinate normalized by the helix lead. Dotted thick lines stand for a wall shear rate of the same value or visualized helix pattern using rheoscopic liquid, see Fig. 3.

(c) left-handed helix (the inclination is opposite to that of the basic CP flow, $n = 1$).

3. Experimental procedure

The experimental set-up, see Fig. 2, and the electrodiffusion method were described in detail in [11]. The inner vertical cylinder ($R_1 = 24.85$ mm) rotates counter clockwise when seen from above. The outer cylinder ($R_2 = 30.95$ mm) is stationary. A volumetric gear pump is used to control axial through flow. It is calibrated by measurement of time spent by the liquid level to overcome an axial (vertical) distance in the gap between cylinders. The liquid is distributed at the bottom through four holes with a diameter of 4 mm on a radius of 20 mm into the gap ($\eta = R_1/R_2 = 0.804$) and flows upwards. It leaves the gap through a spillway in the upper part. The mean flow velocity and the Reynolds number are calculated using the volumetric flow rate provided by the pump.

The test liquid was a 25 mol m^{-3} equimolar potassium hexacyanoferrates (III) and (IV) aqueous solution with 1.5% b.w. K_2SO_4 as supporting electrolyte. The flow was visualized by adding of a few drops of AQ-1000 rheoscopic liquid (Kalliroscope Corp.,U.S.A.).

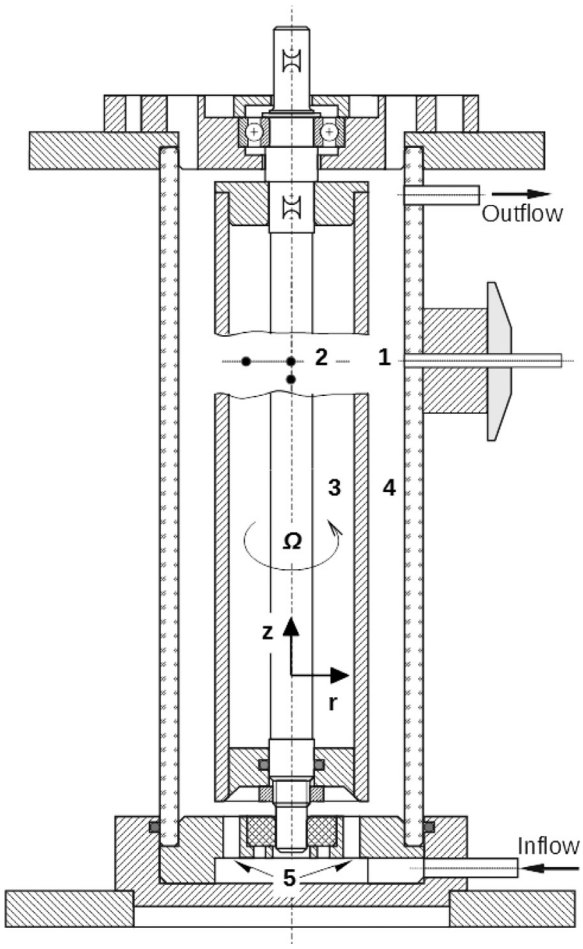

Fig. 2. Experimental set-up. 1-three segment mass transfer (electrodiffusion) probe, 2-array of three simple probes (for detail see Fig. 4), 3-inner cylinder, 4-outer cylinder, 5-liquid distribution through four holes.

The rheoscopic liquid contains small laminae reflecting light in a way that depends on their orientation, which follows the flow direction (Figs 1 and 3).

3.1. Flow visualization and helix characterization

Helices were filmed using a camera with a frequency of 40 frames/s. The parameters such as the helix pitch p, the inclination angle α, the lead l, and the observed velocity U_{OBS} can be estimated from the films. The double right-handed stationary helix (Film 1, $Ta = 159$, $Re = 10.5$, $n = -2$) is shown in Fig. 3 and Film. 1. It should be noted that in order to increase the resolution, the apparatus on this movie is presented in the horizontal position, so the liquid flows from left to right. The helices appear stationary, i.e. the observed axial velocity $U_{OBS} = 0$. However, some non-homogeneity reveal the liquid rotation, especially at the bottom (on the left side in the video).

The axial distance between two helix lines corresponds to two helix pitches, i.e. to the height of the axial cross sections of a pair contra rotating helices or the azimuthal wavelength. $2p$ value of 14.6 mm was obtained as the mean value among eleven helix pairs. It should be noted that in the case of stationary helix, the velocity U_Ω has the same absolute value as U_D but opposite direction.

Helix angle α was estimated from Fig. 3 as the tangent to the helix line in the middle. For an angle of 9°, the lead ($l = 2\pi\ R_2 \tan\alpha$) would be 30.8 mm. As this value is close to $4p$ value red

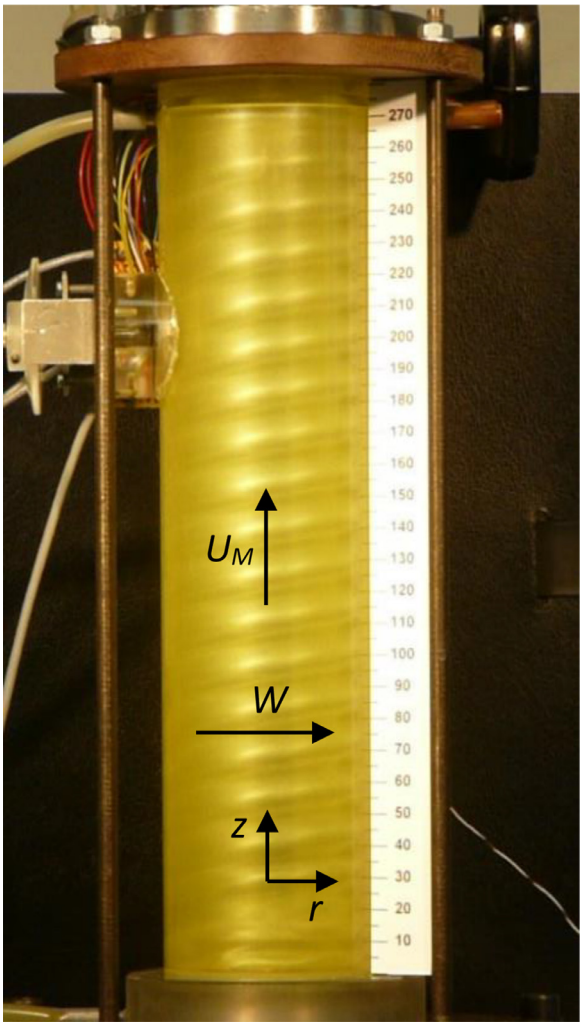

Fig. 3. Stationary right handed double helix (n = -2, Ta = 159, Re = 10.5. The helix pitch p is 7.3 mm, azimuthal wave length = $2p$ =14.6 mm (pair of contra rotating helices) and helix lead l is 29.2 mm (l = $4p$). Flow is visualized using AQ-1000 rheoscopic liquid. W stand for azimuthal velocity of helix and U_M for mean axial velocity of through flow. See Film 1.

from Fig. 3 (29.2 mm), one can conclude that there are two pairs of contra-rotating helices, i.e. double helix, n = -2. Knowing the number of helices, more precise value of α, i.e. 8.54 °, can be calculated from the helix lead l. Video records were also used for evaluating the velocity of axial displacement of helices, U_{OBS}. For this aim, the time of passage of several helices with known pitch was measured. The helix in Film 1 appears stationary, hence U_{OBS} is zero. The error of p and U_{OBS} readings from films, due to uncertainties in the length measurement of several helices or in time measurement of helices passage through a certain point, was smaller than 2%. The estimation of α, using the manual fitting of tangent to the helix pattern in its middle, had an error of 6%.

For Ta around 140–160 and Re around 4–6 and a gap η = 0.848, [12] found what they called “an unusual flow” that consists of helical vortices which appear stationary in both axial and azimuthal directions. The authors also found that the axial wavelength of the stationary helical vortices is *1.7d* and that they have a positive helix angle of 4.5 ° with respect to the flow direction. They stated that such result contradicted previous analytical and experimental results, which indicate that the vortices have a helix angle of opposite sign to that of the basic flow [5,14,18]. As discussed in the previous section, the sign of the helix angle can be either positive

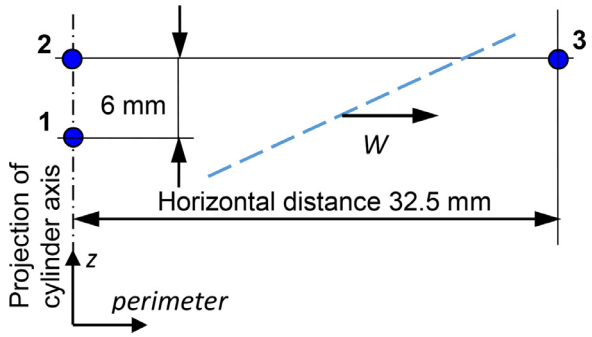

Fig. 4. Three simple mass transfer (electrodiffusion) probes flush mounted in the wall of the outer cylinder. View from the exterior. Dotted line presents iso-wall shear rate or visualized helix (Figs. 1 and 3) moving with azimuthal velocity W.

or negative depending on the winding direction of the helices (see Fig. 1). The effect of inlet system and flow conditions (Ta, Re) can explain the formation of right or left handed helices. Most papers refer to one direction (right or left) helices. In our experimental set-up, the both right and left handed helices were observed at the same Ta and Re without changing the inlet boundary conditions. In this case, the butterfly effect governed helix direction.

Hwang and Yang [8] found an angle of 2.9 ° for a helical vortex (HV) without traveling wave which occurs at Ta = 129 and Re = 24. The authors found traveling waves at a higher Ta than with HV. Two wavelengths were observed for Ta = 167 and Re = 13.1. This type of flow is called “helical wavy vortex” (HWV).

3.2. Measurement of the currents from mass transfer probes

One three-segment probe (ϕ = 0.5 mm) and three simple mass transfer (electrodiffusion) probes (ϕ = 0.1 mm) were flush mounted in the wall of the outer cylinder (namely, probe 1–3). The probe 3 was placed on the same perimeter as the probe 2 at a distance of 32.5 mm, and the probe 1 at a vertical distance of 6 mm from the probe 2 (Fig. 4). The simple probes measured the instantaneous absolute value of the wall shear rate, whereas the three-segment probe measures the components of the wall shear rate in the axial and azimuthal directions. Detailed description of three-segment mass transfer probes and the acquisition of the wall shear rate components can be found in Kristiawan et al. [11].

Passage frequency of moving helices can be measured by any probe. The electric current of stationary helices is constant. Using the observation, that the helix inertia is strong enough to keep their form for more than hundred second after stopping the axial flow, several geometrical and kinematical characteristics (W, Ω_H, n, α, l, p, U_Ω) can be deduced from the currents of the probe array (Fig. 4) measured after stopping axial through flow.

4. Results and discussion

The cross- and auto-correlation of the currents and the distances between the probes were used for the calculation of W, Ω_H, n, α, l, p, U_Ω. The correlations R_{21}, R_{22}, R_{23} between the currents of each two simple probes, for the double right handed stationary helix (Ta = 159, Re = 10.5, n = -2) after stopping axial through flow, are shown in Fig. 5. The time t_{2j} stands for the delay of passage of the wall shear rate array between the probes 2 and j. The periodicity t_{22} is the same for all three currents.

The velocity W was calculated as the distance between the probes 2 and 3 divided by the delay t_{23} (32.5 / 2.35 = 13.8 mm/s). Using the radius R_2, the angular velocity was $\Omega_H = W / R_2$ = 0.446 rad/s. From the known W and the periodicity of current t_{22} we can estimate the number of helices n on the perimeter. The perimeter

Tab. 1
Parameters of helices.
n = -1 single right helix; n = -2 double right helix; n = 1 single left helix; n = 2 double left helix.

Ta	*Re*	*n*	*2p* mm	tan α	tan β	Ω_H rad/s	U_{OBS} mm/s	U_Ω mm/s	U_D mm/s	*V* mm/s	*W* mm/s	AE mm	f_H / f_C	k_t
159	5.05	-1	8.82	0.045	0.075	0.449	0.30	-0.63	0.93	12.6	13.91	364.2	0.20	3.072
159	10.5	-2	14.6	0.150	0.164	0.426	0.00	-1.98	1.94	12.0	13.20	∞	0.00	∞
112	10.5	1	10.9	0.056	0.208	0.334	2.61	0.58	1.94	9.5	10.36	41.2	2.01	0.770
130	10.5	2	12.6	0.129	0.184	0.379	3.51	1.52	1.94	10.7	11.75	39.1	2.03	0.561

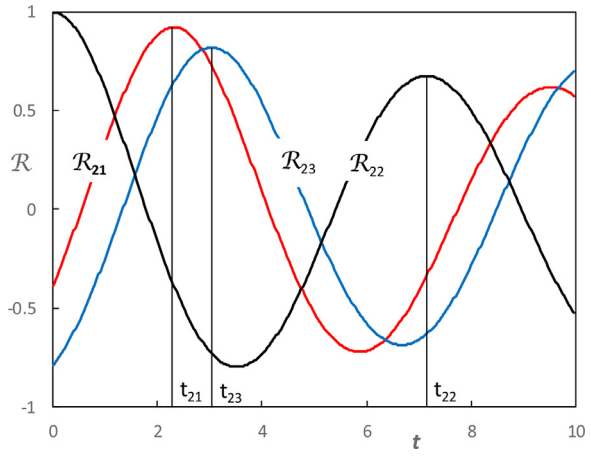

Fig. 5. Correlations between electrodiffusion currents of mass transfer probes 1–3 for stationary right handed double helix (Ta = 159, Re = 10.5, n = -2) measured after stopping axial flow. t_{21} = 2.35 s, t_{23} = 3.08 s, t_{22} = 7.38 s (current period).

divided by the path covered by one helix pair during the time t_{22}: $2\pi\ R_2\ /\ W\ t_{22}$ = 1.91. This result shows that there are two pairs of helices $|n|$ = 2, as n must be an integer.

If the number of helix is known, the rotation rate can be calculated from the frequency of the ED current measured after stopping axial through flow. The single helix (Ta = 177, Re =5.1) in Fig. 12 of Kristiawan et al. [11] had a period of 14 s after stopping axial through flow. As the inner cylinder rotated with a period of 5.9 s, the dimensionless angular velocity $\Omega_H\ /\ \Omega$ = 0.421. The rotation rate can also be deduced from the spectra of ED signal measured after stopping axial through flow.

The helix angle can be calculated from the time t_{21}, the distance between electrodes L_{12} and the azimuthal velocity. For the case Ta = 159, Re = 10.5, n = -2 (Fig. 5): $tan\ \alpha = L_{12}\ /\ (t_{21}\ W)$ = 0.141. The deviation from the value estimated directly from the cinema film ($tan\alpha$ = 0.150) was about 6% larger. The helix lead was calculated as follows: $l = 2\pi\ R_2\ \tan\ \alpha$ = 27.4 mm. The helix pitch p is $p = l\ /\ 2n$ = 6.85 mm. Deviation of this result from a value of 7.3 mm obtained from Film 1 is about 6.2%.

The velocity of axial displacement of helical pattern due to rotation U_Ω (Barber pole effect) was computed as the distance between the probes 2 and 1 divided by t_{21}.

The velocity U_{OBS} was the only parameter evaluated from the currents measured under axial through flow. It was calculated from the distance between the probes 2 and 1 divided by the time t_{21}.

The drifting velocity cannot be measured directly as the helices always rotate. This velocity can be calculated as $U_D = U_{OBS} - U_\Omega$.

The radius of outer cylinder R_2 was used for the calculation of several parameters. This choice is exact for the calculations issuing from the electrodiffusion current or wall shear rate which are measured on the wall. In the visualization study, the radius on which the effects take place can be slightly different from R_2.

The parameters of four typical helices are summarized in Table 1.

4.1. Instantaneous wall shear rate vector fields

It is possible to reconstruct the field of instantaneous wall shear rate when α is different from β. All wall shear rate vectors of the flow manifest themselves along the line AE (Fig. 1b and c).

The three-segment mass transfer probe measures wall shear rate components as a periodical functions of time. The periodicity $T = 2\pi\ f_H$ of signals corresponds to the time of the passage of a selected value between the points A and E in Fig. 1. Since the objective was to obtain the shear rate components distribution at the wall of the outer cylinder, the time series was transformed into space distribution using the fact that this distribution is periodical about one perimeter ($2\pi\ R_2$) and one helix lead l. The area ($2\pi\ R_2$ x l) was divided into k_i = 19 (i = 1..19) and k_j = 10 (j = 1..10) nodes on perimeter (x axis) and helix lead (y axis), respectively. It holds for the shear rate component

$$S_z(i,j) = f_z\left(2\pi\ \left(\frac{i-1}{k_i-1} + \frac{j-1}{k_j-1}\right)\right)$$

The wall shear rate vectors for moving single right-handed helix (n = -1, Ta = 159 and Re = 5.5, Fig. 11 in Kristiawan et al. [11] are shown in Fig. 6a. The arrow lengths correspond to the absolute value of wall shear rate and their direction to the flow direction close to the wall. It is evident that there is only one maximum for each axial distance z/l which corresponds to a single helix. The field of absolute values of wall shear rate, see Fig. 6b, shows even more clearly that there is a single helix. The mean azimuthal component was removed in Fig. 6c. Counter rotating helices can be distinguished from the arrow directions. This approach reveals the oscillation pattern of the wavy vortices better than the instataneous representation. It should be noted that the velocity vectors in Fig. 6c. are scaled by the maximum value of the given case. Therefore, the arrows in c) are longer than that in a).

The field of wall shear rate vectors for the double left-handed helix (n = 2, Ta = 130 and Re = 10.5, Film 5 in Kristiawan et al. [11] is shown in Fig. 6d. The wall shear rate magnitude distribution (Fig. 6e) shows that at any axial distance z/l there are two maxima of wall shear rate, which confirms the presence of double helix. It should be noted that the axial components of wall shear rate are greater than that of the single right-handed helix in Fig. 6a. The vector field with removed mean azimuthal component is shown in Fig. 6f. The axial components are significant without any change of direction towards downwards flow. Fig. 6 also shows that the single helix results in a higher wall shear rate magnitude as compared to the double helix. This could be related to a higher interaction between the helix pairs as compared to the single helix case. The difference in the wall shear rate could also be explained by smaller value of Ta and higher pitch of double helix as compared to single helix.

Right handed helix (n = -1) for Ta = 159 and Re = 5.05: (a) vector field, S_{max} = 20 s^{-1}, (b) absolute value, (c) vector field with the azimuthal mean component removed.

Left handed double helix (n = 2) for Ta = 130 and Re = 10.5: (d) vector field, S_{max} = 7.6 s^{-1}, (e) absolute value, f) vector field with the azimuthal mean component removed.

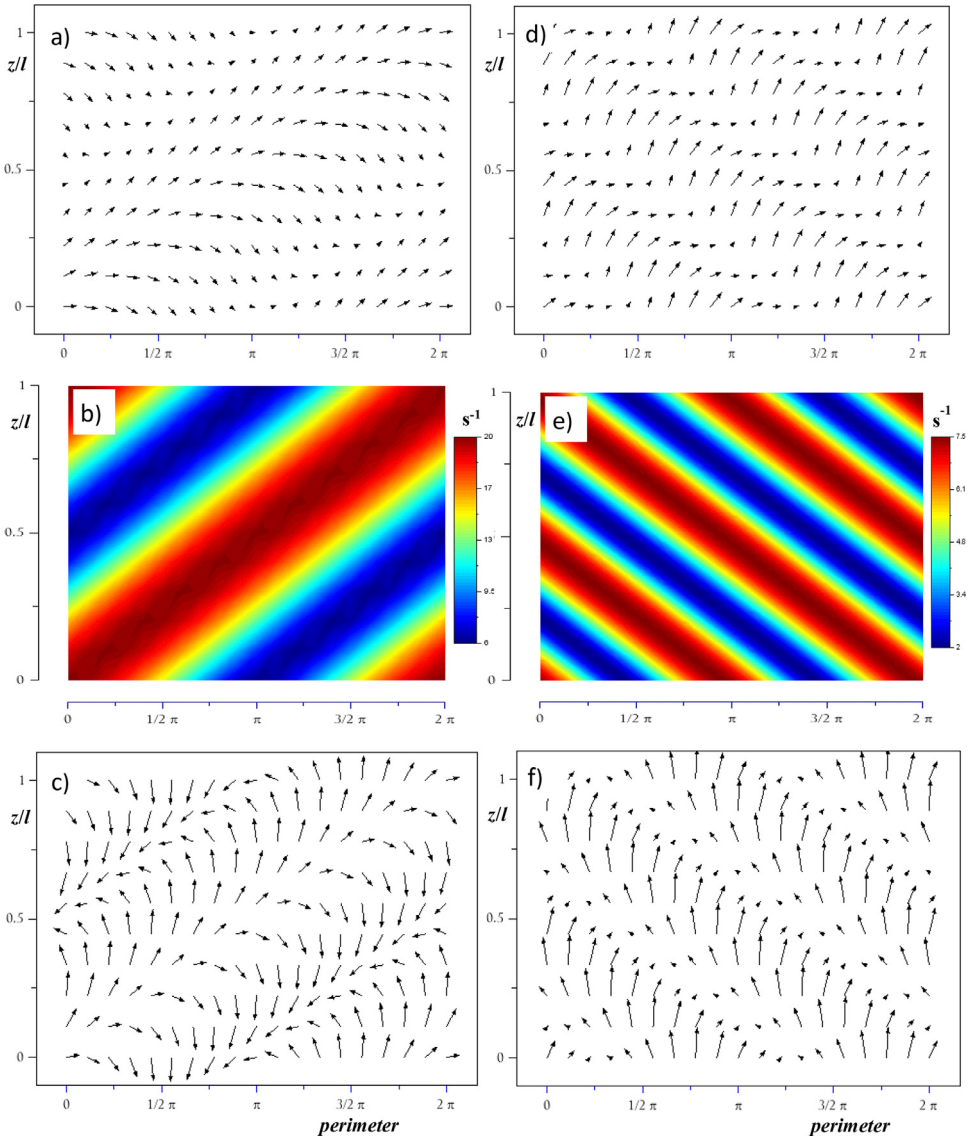

Fig. 6. Instantaneous wall shear rate on perimeter ($2\pi\ R_2$) for one helix lead *l*.

The velocity vectors are scaled by the maximum value of the given case. Therefore, the arrows in (c) and (f) are longer than that in (a) and (d).

4.2. Rotation rate and pitch of helices

The azimuthal and angular velocities W and Ω_H of four typical structures are given in Table 1. The distribution of the rotation rate of helices normalized by that of the inner cylinder (Ω_H/Ω) is shown in Fig. 7. It can be seen that Ω_H/Ω decreases with increasing the Taylor number. The curve shown in the Fig. 6 represents the best fit Ω_H / Ω = 1.069 $Ta^{-0.187}$. It should be also noted that Ω_H/Ω is always greater than 0.35, which is in agreement with that of toroidal vortices [6,10]. The dimensionless rotation rate measured after stopping axial flow can be used for the estimation of number of helix starts. The rate should be lower than 0.5. If the rate is superior to 0.5, there are several helix starts.

It should be noted that the rotation rate of wavy toroidal vortices, Ω_H/Ω = 0.34 [6], was lower than that of the helices. Hwang and Yang [8] found values above 0.4 for both toroidal vortices and helices. This high value for toroidal vortices can be explained by the numerical simulations at Taylor numbers close to the critical levels.

The helix pitch p was assessed from the wall shear rate distribution of the three simple mass transfer probes (see above). The iso-values of the pitch normalized by the gap width p/d for different Taylor and Reynolds numbers are shown in Fig. 8. The pitch of the left-handed helices was close to d, similar to the case of toroidal vortices. The right-handed helices were often axially elongated, with a pitch much larger than d. For example, p/d as high as 1.57 was found for Ta = 177 and Re = 7.4.

The differences in p/d for a given Re are explained by "butterfly effect" of inlet conditions, which was never studied for such a flow. It follows from this figure, that p/d increases with increasing Re. There is a bifurcation at Re = 5 where p/d increases sometimes strongly. The helices with a high p/d values are distorded, as manifested by the course of the axial shear rate component (Fig. 9). The helices with p/d about 1 have the distribution of both the axial and azimuthal shear rate components almost sinusoidal.

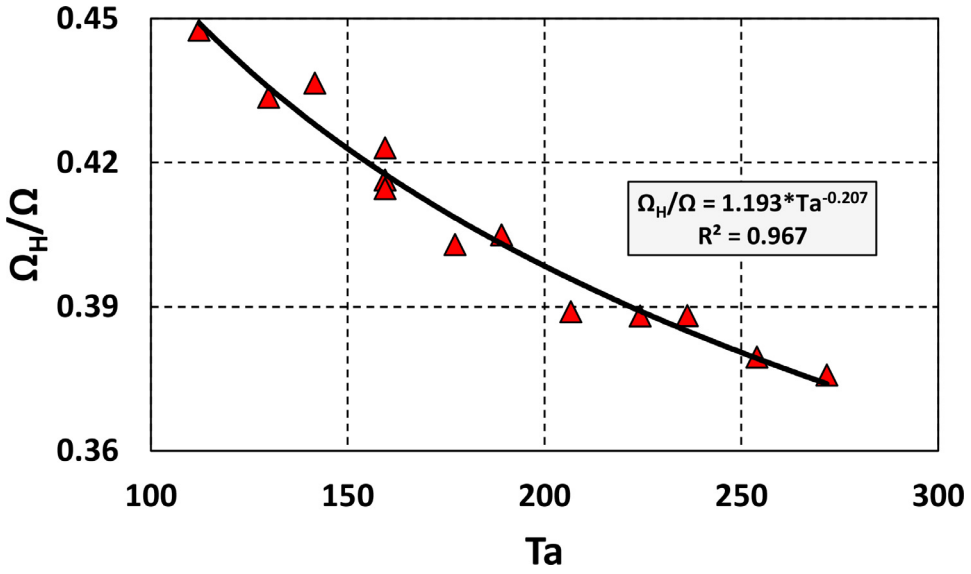

Fig. 7. Dimensionless rotation rate of helices winding in the same direction as the base flow (right-handed). Curve stand for the best fit $\Omega_H / \Omega = 1.069\ Ta^{-0.207}$, $R^2 = 0.967$.

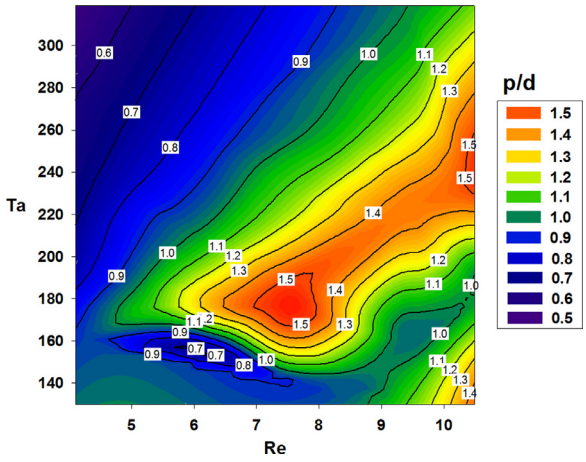

Fig. 8. Dimensionless helix pitch of right-handed helices as function of *Re* and *Ta*.

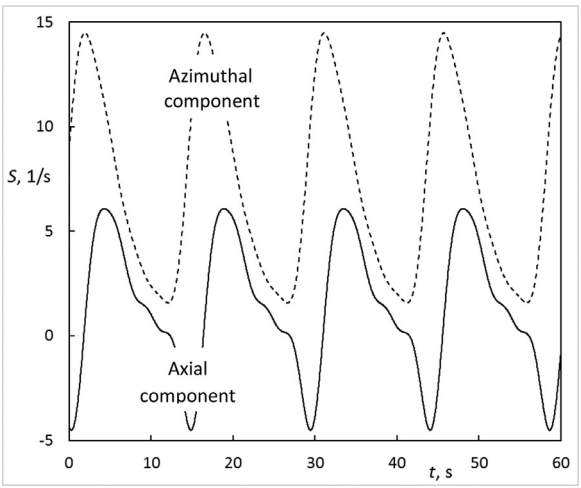

Fig. 9. Wall shear rate components of right handed helix for $Re = 7.4$, $Ta = 177.3$ and $p/d = 1.57$.

4.3. Observed velocity of axial displacement of helices and frequency of helix passage

The superposition of the drifting velocity U_D and the velocity due to helix rotation U_Ω is elucidated on the moving right helix, Table 1, $n = -1$, $Re = 5.05$, $Ta = 159$. A frequency of 0.071 s^{-1} was estimated from the period of 14 s after stopping axial through flow. The downward velocity due to the helix rotation was equal to the helix frequency multiplied by too helix pitch (8.82 mm) and the number of helix ($n = -1$). The resulting value ($U_\Omega = -0.626$ mm/s) agrees well with the value - 0.645 mm/s obtained from the film. It is suggested that the effect of axial through flow on the helices was the same as on the toroidal vortices, i.e. their drifting velocity was 1.12 times the mean axial velocity. Under this assumption the helix moved at a velocity $U_D = 0.934$ mm/s. The observed velocity is the sum of this velocity and the velocity due to the rotation U_Ω (barber-pole effect), i.e. $U_{OBS} = 0.308$ mm/s which agrees well with the value obtained from the film (0.303 mm/s). The observed velocity can also be calculated from the frequency of the ED current measured under axial through flow, multiplied by the axial wave length $2p$: $U_{OBS} = 0.298$ mm/s. The difference in the axial velocity using the three methods was less than 4%.

The observed velocity of axial displacement of structures (U_{OBS}) normalized with the mean velocity of the axial through flow (U_M) is shown in Fig. 10. It is obvious that this velocity does not depend on Taylor number. The Taylor vortices moves with a non-dimensional velocity of about 1.12, which is close to the value calculated using the results of Recktenwald et al. [16]. The present results are also in agreement with those of Snyder [17] and Hwang and Yang [8]. It should be noted that the right-handed helices appeared stationary, $U_{OBS} = 0$. A few helices moved upward at a dimensionless velocity of between 0.36 and 0.54. The left-handed helices moved always upward at a velocity in the interval 1.5–2. After the cessation of axial through flow, the velocity U_{OBS} of the stationary right handed helices was downward with an absolute value equal to U_D before the flow cessation.

The frequency of helix passage was obtained under axial through flow, either from the period of electrodiffusion current or by counting the passage of structures through a fix point in the cinema films. This frequency for left-handed helices, normalized with the inner cylinder frequency, has entire values of 1 or 2. For $Re > 10$ and low *Ta* numbers this value is 2 as shown in the Fig. 11.

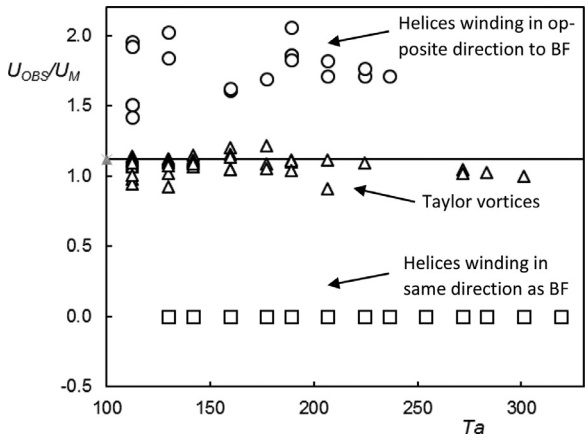

Fig. 10. Dimensionless apparent velocity. Triangles represent Taylor vortices; rectangles indicate helices winding in the same direction and circles correspond to helices winding in the opposite direction to the base flow (BF). The horizontal red line represents the value 1.12 obtained for Taylor vortices at $\eta = 0.83$ by Recktenwald et al. [16].

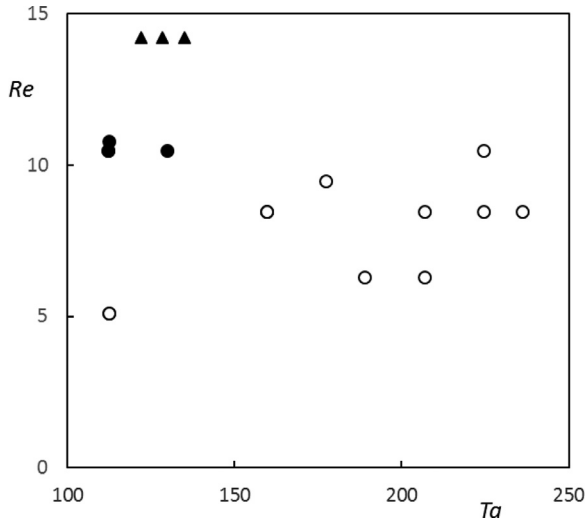

Fig. 11. Frequency of passage of left handed helices normalized by that of the inner cylinder is equal to: ● two, ○ one, ▲ two [21].

Wereley and Lueptow [21] found the same value for a left hand helices in the ranges Re = 14-23, Ta = 120–150. However for $Re < 10$, it is found that the helix passage frequency is equal to the cylinder rotation frequency within a maximum difference of 7%, $f_h/f_c \in (0.93,\ 1.07)$. This frequency does not depend on the Ta number.

5. Conclusion

Helical vortices winding in the same (right-handed) or opposite direction (left-handed) to the base Taylor-Couette-Poiseuile flow were studied at low Taylor and Reynolds numbers. The motion of helical structures is composed of azimuthal velocity induced by the inner cylinder rotation and drifting velocity due to superposed axial through flow. The kinematical and geometrical parameters of helical vortices were obtained from flow visualizations and the wall shear rate measurements. The vector field of wall shear rate on the outer cylinder was reconstructed using a three-segment mass transfer probe.

Flow visualizations showed that the time averaged velocity vectors are in the same quadrant (0–90 °) for both helices winding in the same direction and opposite direction to the base flow. In addition, the axial velocity due to helix rotation depends on azimuthal velocity, helix lead and number of helix starts. The helices look like spiral tubes which rotate in the meridional plane in contra sense, but there is no net flow through these tubes.

The mass transfer measurement showed that the axial component of the wall shear rate of the left-handed helices is greater than that of the right-handed helices. The helices rotate around the cylinder axis at an angular velocity inferior to that of the inner cylinder (0.37–0.45). The helices move axially at a drifting velocity superior to that of mean axial through flow (multiple of 1.12). The observed axial velocity of helices is composed of the drifting velocity and the velocity resulting of helix rotation (barber pole effect). These velocities have the opposite or same direction in the case of helices winding in the same or opposite direction to the base flow, respectively.

It was also found that the right-handed helices were axially elongated for wide range of Re and Ta. This was illustrated from a pitch much larger than the gap width and could be explained by "butterfly effect" of inlet conditions. The resulting helices are distorded, which was illustrated by the variation of the axial shear rate.

The obtained results are helpful for verification of numerical simulations of rotational flows.

The effect of higher values of Ta and Re on the flow between cylinders will be studied in the future.

Declaration of Competing Interest

None.

Supplementary materials

Supplementary material associated with this article can be found, in the online version, at doi:10.1016/j.ijheatmasstransfer.2021.121938.

Appendix

The helix inclination angle α depends on the helix lead and the perimeter of the outer cylinder.

$$tan\ \alpha = \frac{l}{2\pi R_2}$$

The angle β is a function of the drifting and azimuthal velocity U_D and W, respectively.

$$tan\ \beta = \frac{U_D}{W}$$

The drifting velocity cannot be measured directly because helices always rotate. The analysis of the observed velocity U_{OBS} has shown that the U_D of helices is the same as that of toroidal vortices, i.e. about 1.12 multiple of the mean axial velocity. The azimuthal velocity W was calculated from the measured period after stopping axial through flow. The axial velocity due to the helix rotation U_Ω was expressed as the frequency of helix rotation multiplied by his lead. Using these hypothesis, the equation $U_{OBS} = U_\Omega + U_D$ was fulfilled with an error smaller than 4%.

The period of helices is equal to the distance AE divided by the velocity V.

$$t_{left} = \frac{\overline{AE}}{V} = \frac{\overline{AE\ sin\beta}}{U_D} = \frac{l}{nU_D}\frac{cos\alpha\ sin\beta}{\sin(\alpha+\beta)}$$

$$= \frac{l}{nU_D}\frac{cos\alpha\ sin\beta}{\sin\alpha\ cos\beta + cos\alpha\ sin\beta}$$

$$= \frac{l}{nU_D}\ \frac{1}{1+\frac{\sin\alpha\ cos\beta}{cos\alpha\ sin\beta}} = \frac{l}{nU_D}\ \frac{1}{1+\frac{tan\ \alpha}{tan\ \beta}} = \frac{l}{nU_D}\ k_{t,l}$$

$$t_{right} = \frac{\overline{AE}}{V} = \frac{\overline{AE\ sin\beta}}{U_D} = \frac{l}{|n|U_D}\frac{cos\alpha\ sin\beta}{\sin(\beta-\alpha)}$$
$$= \frac{l}{|n|U_D}\frac{cos\alpha\ sin\beta}{\sin\beta\ cos\alpha - cos\beta\ sin\alpha}$$
$$= \frac{l}{|n|U_D}\ \frac{1}{1-\frac{\sin\alpha\ cos\beta}{cos\alpha\ sin\beta}} = \frac{l}{|n|U_D}\frac{1}{1-\frac{tan\ \alpha}{tan\ \beta}} = \frac{l}{|n|U_D}\ k_{t,r}$$

where k_t is the coefficient proper to the right ($k_{t,r} > 1$) or left handed ($k_{t,l} < 1$) helix. The term l / $|n|$ U_D represents the period of passage of toroidal vortices where l is equal to their azimuthal wavelength.

It follows that:

$$t_{right} > \frac{l}{|n|U_D} > t_{left}$$

CRediT authorship contribution statement

M. El Hassan: Writing – original draft, Data curation, Formal analysis, Writing – review & editing. **V. Sobolik:** Conceptualization, Methodology, Supervision, Writing – review & editing. **A. Chamkha:** Writing – review & editing. **M. Kristiawan:** Writing – original draft, Data curation.

References

[1] S. Altmeyer, C.H. Hoffmann, M. Lücke, Islands of instability for growth of spiral vortices in the Taylor-Couette system with and without axial through flow, Phys. Rev. E 84 (2011) 046308.
[2] N. Abcha, O. Crumeyrolle, A.B. Ezersk, I. Mutabazi, Velocity field of the spiral vortex flow in the Couette-Taylor system, Eur. Phys. J. E 35 (2013) 20.
[3] K. Bühler, Instabilitäten spiralförmiger strömungen im zylinderspalt, ZAAM 64 (1984) 180–184.
[4] S. Chandrasekhar, The hydrodynamic stability of viscid flow between coaxial cylinders, Proc. Nat. Acad. Sci. 46 (1960) 141–151.
[5] K.C. Chung, K.N. Astill, Hydrodynamic instability of viscous flow between rotating coaxial cylinders with fully developed axial through flow, J. Fluid Mech. 81 (1977) 641–655.
[6] D. Coles, Transition in circular Couette flow, J. Fluid Mech. 21 (1965) 385–425.
[7] R.C. DiPrima, The stability of a viscous fluid between rotating cylinders with an axial through flow, J. Fluid Mech. 9 (1960) 621–631.
[8] J.Y. Hwang, K.S. Yang, Numerical study of Taylor –Couette flow with an axial through flow, Comput. Fluid. 33 (2004) 97–118.
[9] K. Kataoka, H. Doi, T. Komai, Heat/mass transfer in Taylor vortex flow with constant axial through flow rates, Int. J. Heat Mass Transf. 20 (1977) 57–63.
[10] G.P. King, Y. Li, W. Lee, H.L. Swinney, P.S. Marcus, Wave speeds in Taylor vortex flow, J. Fluid Mech. 141 (1984) 365–390.
[11] M. Kristiawan, M. El Hassan, A. El Faye, V. Sobolík, Experimental investigation of Taylor-Couette-poiseuille flow at low Taylor and Reynolds numbers, PLOS ONE (2019), doi:10.1371/journal.pone.0212728.
[12] R.M. Lueptow, A. Docter, K. Min, Stability of axial through flow in an annulus with a rotating inner cylinder, Phys. Fluid. A 4 (1992) 2446–2455.
[13] D. Martinand, E. Serre, R.M. Lueptow, Absolute and convective instability of cylindrical Couette flow with axial and radial flows, Phys. Fluid. 21 (2009) 1–13 104102.
[14] B.S. Ng, E.R. Turner, "On the linear stability of spiral flow between rotating cylinders", Proc. R. Soc. Lond. Ser. A 382 (1982) 83.
[15] G. Raguin, J.G. Georgiadis, Kinematics of the stationary helical vortex mode in Taylor-Couette-Poiseuille flow, J. Fluid Mech. 516 (2004) 125–154.
[16] A. Recktenwald, M. Lucke, H.W. Muller, Taylor vortex formation in axial through-flow: linear and weakly nonlinear analysis, Phys. Rev. E 48 (1993) 4444–4454.
[17] H.A. Snyder, Experiments on the stability of spiral flow at low axial Reynolds numbers, Proc. R. Soc. Lond. A 265 (1962) 198–214.
[18] H.A. Snyder, Experiments on the stability of two types of spiral flow, Ann. Phys. 31 (1965) 292–313.
[19] D.I. Takeuchi, D.F. Jankowski, A numerical and experimental investigation of the stability of spiral Poiseuille flow, J. Fluid Mech. 102 (1981) 101–126.
[20] S. Vedantam, J.B. Joshi, Annular centrifugal contactors–a review, Chem. Eng. Res. Des. 84 (A7) (2006) 522–542.
[21] S.T. Wereley, R.M. Lueptow, Velocity field for Taylor–Couette flow with an axial through flow, Phys. Fluid. 11 (1999) 3637–3649.